INTERNATIONAL JOURNAL OF
NUMERICAL ANALYSIS AND MODELING, *SERIES B*
Volume 3, Number 3, Pages 330–344

MULTIPHYSICS AND MULTIMETHODS PROBLEM OF ROTATIONAL GLASS FIBER MELT-SPINNING

NICOLE MARHEINEKE[†], JALO LILJO[‡], JAN MOHRING[‡], JOHANNES SCHNEBELE[‡], AND RAIMUND WEGENER[‡]

Abstract. Glass wool manufacturing is a multiphysics problem which requires the understanding of the rotational melt-spinning of ten thousands of viscous thermal slender jets by fast air streams. Due to its high complexity an uniform numerical treatment is impossible. In this work we present a multimethods approach that is based on an asymptotic modeling framework of slender-body theory, homogenization and surrogate models. The algorithm weakly couples melting and spinning phases via iterations. The possibility of combining commercial software and self-implemented code yields satisfying efficiency off-the-shelf. The simulation results are very promising and demonstrate the applicability and practical relevance of our approach for ongoing optimization strategies of the production processes.

Key words. Rotational spinning, viscous thermal jets, fluid-structure interactions, fluid dynamics, structure mechanics, heat transfer, slender-body theory, Cosserat rods, drag models

1. Introduction

A rigorous understanding of the rotational spinning of viscous thermal jets exposed to gravity and/or aerodynamic forces is of interest in many industrial applications, e.g. glass/polymer fiber spinning/tapering [22, 14], pellet manufacturing [8, 21], technical textile production [2, 3]. This work deals with glass wool manufacturing. Rotational spinning processes consist in general of two regimes: melting and spinning. As a representative example we focus on a specific melt-spinning process whose set-up is illustrated in Figure 1. Here, glass is heated in a stove from which the melt is led to a centrifugal disk. The walls of the disk are perforated by ten thousands of tiny holes that are placed equidistantly in a spinning row with tens of rows over height. Emerging from the rotating disk via continuous extrusion, the liquid jets grow and move due to viscosity, surface tension, gravity and aerodynamic forces. There are two air flows interacting with the arising glass fiber curtain: a downwards-directed hot burner flow that keeps the jets near the spinning nozzles warm and thus extremely viscous and shapeable as well as a highly turbulent cold cross-stream that stretches and finally cools them down such that the glass fibers become hardened. These fibers yield the basic fabric for the final glass wool product. For the quality assessment of the fabrics the properties of the single spun fibers, i.e. homogeneity and slenderness, play an important role. A long-term objective in industry is the optimal design of the manufacturing process with respect to desired product specifications and low production costs. Therefore, it is necessary to model, simulate and control the whole process.

The goal of this paper is the first numerical simulation of the whole process, regarding all effects. The manufacturing process is a multiphysics problem whose uniform numerical treatment is impossible because of the enormous complexity.

Received by the editors May 5, 2011 and, in revised form, March 2, 2012.
2000 *Mathematics Subject Classification.* 76-xx, 34B08, 41A60, 65L10, 65Z05.

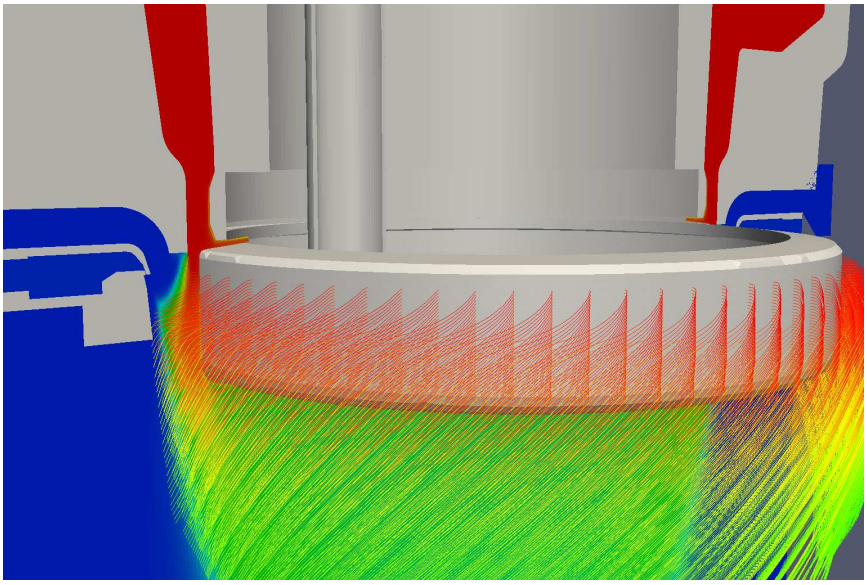

FIGURE 1. Specific rotational melt-spinning process of our industrial partner with 30 000 glass jets. Only every tenth jet is plotted here. The temperatures of air flow and fiber jets are visualized by the color map that ranges from 30°C (blue) to 1500°C (red).

Hence, we follow the idea to handle it as a multimethod problem by deriving adequate models and methods for the separate regimes and coupling them appropriately (see [17] for a similar strategy in the field of nonwoven production). In this sense and contents, the spinning phase has already been modeled and investigated in [3]. In the spinning phase the liquid viscous glass jets are stretched by the surrounding air flow to form long thin fibers of slenderness ratio $\delta = d/l \ll 1$ (with jet diameter d and length l) that lie dense in an arising curtain. To predict the resulting fiber/fabric properties, the fiber-fluid interactions have to be considered. This involves, in principle, the solution of a three-dimensional multiscale-multiphase problem. However, in view of thousands of slender glass jets and fast air streams direct numerical simulation as well as numerical approaches (like embedded domain approaches or immersed boundary methods) are not applicable. Thus, an asymptotic coupling concept has been developed in [3]. Treating the glass jets as viscous thermal Cosserat rods, the multiscale problem is tackled by help of momentum (drag) and heat exchange models that are derived on basis of slender-body theory and homogenization. A robust and efficient weak iterative algorithm makes then the simulation of the industrial spinning phase with its fiber-fluid interactions possible. In that work the melt conditions at the nozzles (i.e. velocity and temperature) and the temperature of the disk wall which act as boundary conditions for glass jets and air flow computations of the spinning phase as well as the disk geometry itself were assumed to be known.

But, in view of the design of the whole manufacturing process the melting phase must certainly be taken into account in modeling and simulation. It deals with the highly viscous melt coming from the stove and creeping in the centrifugal disk to the perforated walls. Melting and spinning phases obviously influence each other. On one hand the conditions at the spinning rows are crucially affected by the melt

distribution in the centrifugal disk and by the outer burner air flow. On the other hand the air flow and the arising heat distortion of the disk are affected by the spun jet curtain. This paper aims for the modeling and simulation of the whole manufacturing process for the first time. Proceeding from the asymptotic modeling framework of [3] for the spinning phase, we extend it with respect to the melting phase for which we develop a simplified model including the disk mechanics. The disk mechanics determines the disk geometry and hence the air flow domain. The models associated to the subproblems of both phases couple via their boundary conditions. Whereas the melting phase provides the information of the glass jets' velocity and temperature at the spinning nozzles and of the disk wall's temperature for the air flow, the spinning phase yields the heat flux at the centrifugal disk due to air flow and jet curtain. This is used in the numerical realization where we perform the melting and spinning computations iteratively.

The paper is structured with respect to the two subproblems of spinning und melting phases, their separate modeling and their common iterative numerical handling. In Section 2 we start with an overview of the asymptotic modeling framework [3] for the fiber-fluid interactions in the spinning phase. We introduce the viscous thermal Cosserat rod system and the compressible Navier-Stokes equations for glass jets and air flow, respectively, and present the models for the momentum and energy exchange: drag and Nusselt function. Since the modeling of jet dynamics and drag has been a challenging topic of research for decades and it is still, an enormous amount of literature exists in this field and we pay special attention to the embedding of the used slender-body theory and results into recent studies and history. In Section 3 we deal with the modeling of the melting phase. We treat the creeping melt in the centrifugal disk as Stokes flow and study mechanics and heat transfer of the disk. The specific set-up of the industrial melt-spinning process allows for a number of model simplifications, e.g. assumptions of rotational invariance and stationarity which implies the reduction of dimensions and dependencies. In Section 4 we propose a weak iterative scheme that is adequate for the full problem. It offers the possibility of combining commercial software and self-implemented code which yields satisfying efficiency off-the-shelf. Simulation results for a special manufacturing adjustment demonstrate the applicability and practical relevance of our approach for ongoing optimization strategies.

2. Modeling of spinning phase: fiber-fluid interactions

We are interested in the spinning of ten thousands of slender glass jets by fast air streams. The glass jets form a kind of curtain that interact and crucially affect the surrounding air. For the determination of the fluid-fiber interactions we use an asymptotic coupling concept [3] for slender bodies and fluid flows that is based on drag force and heat exchange models. Considering slender jets, there are two classes of asymptotic one-dimensional models, i.e. string and rod models [1]. Whereas the string models consist of balance equations for mass and linear momentum, the more complex rod models contain also an angular momentum balance, [11, 32]. A string model for the jet dynamics was derived in a slender-body asymptotics from the three-dimensional free boundary value problem given by the incompressible Navier-Stokes equations in [18]. Accounting for inner viscous transport, surface tension and placing no restrictions on either the motion or the shape of the jet's center-line, it generalizes the previously developed string models for straight [7, 9, 10] and curved [21, 31, 20] center-lines. However, already in the stationary case the applicability of the string model turns out to be restricted to

certain parameter ranges [13, 2] because of a non-removable singularity that comes from the deduced boundary conditions. These limitations can be partly overcome by a modification of the boundary conditions, i.e. the release of the condition for the jet tangent at the nozzle in favor of an appropriate interface condition, [15, 16, 4]. This involves two string models that exclusively differ in the closure conditions. For gravitational spinning they cover the whole parameter range, but in the presence of rotations there exist still small parameter regimes where none of them works. A rod model that allows for stretching, bending and twisting was proposed and analyzed in [23, 24] for the coiling of a viscous jet falling on a rigid substrate. Based on these studies and embedded in the special Cosserat theory a modified incompressible isothermal rod model was developed and investigated for rotational spinning in [2, 4]. It shows its superiority to the string by covering the whole parameter range, (similar as in the application of a fluid-mechanical "sewing machine" [25]). By containing the slenderness parameter δ explicitely in the angular momentum balance, the rod model is no asymptotic model of zeroth order. Since its solutions converge to the respective string solutions in the slenderness limit $\delta \to 0$, it can be considered as δ-regularized model, [4]. For the considered industrial spinning set-up, temperature dependencies and aerodynamic forces were included in the rod model, [3]. The air drag model applied on the moving curved jets stems thereby from [19], it combines Oseen and Stokes theory [29, 5, 6], Taylor heuristic [28] and numerical simulations. According to the experimental validation, it is applicable for all air flow regimes and incident flow directions. The aerodynamic heat source that is based on the Nusselt number [30] is modeled correspondingly. For a flow around a slender straight cylinder with circular cross-sections these relations are well studied in literature, for a survey on the theoretical, numerical and experimental investigations see e.g. [19, 27, 33, 26] and references within. Within this slender-body framework, the interactions (two-way coupling) between glass jets and air flow are realized by inserting the homogenized drag and heat source terms in the balance equations of the air flow, following the principle that action equals reaction.

In this section we briefly outline the asymptotic coupling concept of viscous thermal Cosserat rods and compressible Navier-Stokes equations. Thereby, we choose an invariant formulation in the three-dimensional Euclidian space $\mathbb{E}^3$. For details we refer to [3] and references within. Then, we explain the simplifications on the modeling framework that can be done for the specific industrial spinning set-up.

2.1. Asymptotic framework for slender-body dynamics in fluid flows. In the special Cosserat rod theory [1], a fiber jet is represented by two constitutive elements: a curve specifying the position $\mathbf{r} : Q \to \mathbb{E}^3$ and an orthonormal director triad $\{\mathbf{d_1}, \mathbf{d_2}, \mathbf{d_3}\} : Q \to \mathbb{E}^3$ characterizing the orientation of the cross-sections, where $Q = \{(s,t) \in \mathbb{R}^2 | s \in I(t) = [0, l(t)], t > 0\}$ with arclength parameter s and time t. Apart from these quantities, the viscous thermal rod model describes the variables of generalized curvature $\boldsymbol{\kappa}$, convective speed u, cross-section A, linear velocity $\mathbf{v}$, angular velocity $\boldsymbol{\omega}$, temperature T and normal contact forces $\mathbf{n} \cdot \mathbf{d}_\alpha$, $\alpha = 1, 2$. It consists of four kinematic and four dynamic equations, i.e. balance laws for mass (cross-section), linear and angular momentum and temperature,

$$
\begin{aligned}
\partial_t \mathbf{r} &= \mathbf{v} - u\mathbf{d_3} \\
\partial_t \mathbf{d_i} &= (\boldsymbol{\omega} - u\boldsymbol{\kappa}) \times \mathbf{d_i} \\
\partial_s \mathbf{r} &= \mathbf{d_3} \\
\partial_s \mathbf{d_i} &= \boldsymbol{\kappa} \times \mathbf{d_i}
\end{aligned}
\tag{1}
$$

$$\begin{aligned}\partial_t A + \partial_s(uA) &= 0\\ \rho\left(\partial_t(A\mathbf{v}) + \partial_s(uA\mathbf{v})\right) &= \partial_s\mathbf{n} + \rho A g\mathbf{e_g} + \mathbf{f}_{air}\\ \rho\left(\partial_t(\mathbf{J}\cdot\boldsymbol{\omega}) + \partial_s(u\mathbf{J}\cdot\boldsymbol{\omega})\right) &= \partial_s\mathbf{m} + \mathbf{d_3}\times\mathbf{n}\\ \rho c_p\left(\partial_t(AT) + \partial_s(uAT)\right) &= q_{rad} + q_{air}\end{aligned}$$

supplemented with an incompressible geometrical model of circular cross-sections with diameter d

$$\mathbf{J} = I(\mathbf{d_1}\otimes\mathbf{d_1} + \mathbf{d_2}\otimes\mathbf{d_2} + 2\mathbf{d_3}\otimes\mathbf{d_3}), \qquad I = \frac{\pi}{64}d^4, \qquad A = \frac{\pi}{4}d^2$$

as well as viscous material laws for the tangential contact force $\mathbf{n}\cdot\mathbf{d_3}$ and contact couple $\mathbf{m}$

$$\mathbf{n}\cdot\mathbf{d_3} = 3\mu A\partial_s u, \qquad \mathbf{m} = 3\mu I(\mathbf{d_1}\otimes\mathbf{d_1} + \mathbf{d_2}\otimes\mathbf{d_2} + \frac{2}{3}\mathbf{d_3}\otimes\mathbf{d_3})\cdot\partial_s\boldsymbol{\omega}.$$

Rod density ρ and heat capacity c_p are assumed to be constant. The temperature-dependent dynamic viscosity μ is modeled according to the Vogel-Fulcher-Tamman relation [30]. The external loads rise from gravity $\rho A g\mathbf{e_g}$ with gravitational acceleration g and aerodynamic forces $\mathbf{f}_{air}$. In the temperature equation inner friction and heat conduction are neglected in favor of radiation q_{rad} and aerodynamic heat sources q_{air}. The radiation effect depends on the geometry of the plant and is incorporated in the system by help of the simple model $q_{rad} = \varepsilon\sigma\pi d(T_{ref}^4 - T^4)$ with emissivity ε, Stefan-Boltzmann constant σ and reference temperature T_{ref}. Appropriate initial and boundary conditions close the rod system.

A compressible air flow in the space-time domain $\Omega_t = \{(\mathbf{x},t)|\mathbf{x}\in\Omega\subset\mathbb{E}^3, t>0\}$ is described by density $\rho_\star$, velocity $\mathbf{v}_\star$, temperature $T_\star$. Its model equations consist of the balance laws for mass, momentum and energy,

$$\begin{aligned}\partial_t\rho_\star + \nabla\cdot(\mathbf{v}_\star\rho_\star) &= 0\\ \partial_t(\rho_\star\mathbf{v}_\star) + \nabla\cdot(\mathbf{v}_\star\otimes\rho_\star\mathbf{v}_\star) &= \nabla\cdot\mathbf{S}_\star^T + \rho_\star g\mathbf{e_g} + \mathbf{f}_{jets}\\ \partial_t(\rho_\star e_\star) + \nabla\cdot(\mathbf{v}_\star\rho_\star e_\star) &= \mathbf{S}_\star : \nabla\mathbf{v}_\star - \nabla\cdot\mathbf{q}_\star + q_{jets}\end{aligned} \tag{2}$$

supplemented with the Newtonian stress tensor $\mathbf{S}_\star$, the Fourier law for heat conduction $\mathbf{q}_\star$

$$\mathbf{S}_\star = -p_\star\mathbf{I} + \mu_\star(\nabla\mathbf{v}_\star + \nabla\mathbf{v}_\star^T) + \lambda_\star\nabla\cdot\mathbf{v}_\star\mathbf{I}, \qquad \mathbf{q}_\star = -k_\star\nabla T_\star,$$

as well as thermal and caloric equations of state of a ideal gas

$$p_\star = \rho_\star R_\star T_\star, \qquad e_\star = \int_0^{T_\star} c_{p\star}(T)\mathrm{d}T - \frac{p_\star}{\rho_\star}$$

with pressure $p_\star$ and inner energy $e_\star$. The specific gas constant for air is denoted by $R_\star$. The temperature-dependent viscosities $\mu_\star$, $\lambda_\star$, heat capacity $c_{p\star}$ and heat conductivity $k_\star$ can be modeled by standard polynomial laws, see e.g. [12, 30]. External loads rise from gravity $\rho_\star g\mathbf{e_g}$ and forces due to the immersed glass fiber jets $\mathbf{f}_{jets}$. These fiber jets also imply a heat source q_{jets} in the energy equation. Appropriate initial and boundary conditions close the system.

The two-way coupling of (1) and (2) is performed by help of drag forces and heat sources. Taking into account the conservation of momentum and energy, $\mathbf{f}_{air}$ and $\mathbf{f}_{jets}$ as well as q_{air} and q_{jets} satisfy the principle that action equals reaction and obey common underlying relations. Hence, the fiber-fluid interactions are realized by two exchange functions, i.e. dimensionless drag force $\boldsymbol{F}$ and Nusselt number Nu. Let $\boldsymbol{\Psi}$ and $\boldsymbol{\Psi}_\star$ represent all glass jet and air flow quantities, respectively. Thereby,

$\mathbf{\Psi}_\star$ is the spatially averaged solution of (2), this delocation is necessary to avoid singularities in the coupling.

The (line) drag force acting on a slender body

$$\mathbf{f}_{air}(s,t) = \boldsymbol{\mathcal{F}}(\mathbf{\Psi}(s,t), \mathbf{\Psi}_\star(\mathbf{r}(s,t),t)), \qquad \boldsymbol{\mathcal{F}}(\mathbf{\Psi}, \mathbf{\Psi}_\star) = \frac{\mu_\star^2}{d\rho_\star}\, \boldsymbol{F}\left(\mathbf{d_3}, \frac{d\rho_\star}{\mu_\star}(\mathbf{v}_\star - \mathbf{v})\right)$$

is caused by friction and inertia. It depends on material and geometrical properties as well as on the specific inflow situation. The number of dependencies reduces to two by non-dimensionalizing which yields the dimensionless drag force $\boldsymbol{F}$ in dependence on the jet orientation (tangent) and the dimensionless relative velocity between air flow and glass jet. A specific inflow situation $(\boldsymbol{\tau}, \mathbf{w})$ with orientation $\boldsymbol{\tau}$ and velocity $\mathbf{w}$ induces an orthonormal basis $\{\mathbf{n}, \mathbf{b}, \boldsymbol{\tau}\}$

$$\mathbf{n} = \frac{\mathbf{w} - w_\tau \boldsymbol{\tau}}{w_n}, \qquad \mathbf{b} = \boldsymbol{\tau} \times \mathbf{n}, \qquad w_\tau = \mathbf{w} \cdot \boldsymbol{\tau}, \qquad w_n = \sqrt{\mathbf{w}^2 - w_\tau^2},$$

assuming $\mathbf{w} \nparallel \boldsymbol{\tau}$. In this basis, the force $\boldsymbol{F} : S^2 \times \mathbb{E}^3 \to \mathbb{E}^3$ is given by

$$\boldsymbol{F}(\boldsymbol{\tau}, \mathbf{w}) = F_n(w_n)\mathbf{n} + F_\tau(w_n, w_\tau)\boldsymbol{\tau} \tag{3}$$

$$F_n(w_n) = w_n^2\, c_n(w_n) = w_n\, r_n(w_n), \qquad F_\tau(w_n, w_\tau) = w_\tau\, w_n\, c_\tau(w_n) = w_\tau\, r_\tau(w_n)$$

according to the Independence Principle. The differentiable normal and tangential drag functions c_n, c_τ are modeled as

$$c_n(w_n) = \begin{cases} \frac{4\pi}{S w_n}\left[1 - w_n^2 \frac{S^2 - S/2 + 5/16}{32 S}\right], & w_n < w_1 \\ \exp\left(\sum_{j=0}^{3} p_{n,j} \ln^j w_n\right), & w_1 \le w_n \le w_2 \\ \frac{2}{\sqrt{w_n}} + 0.5, & w_2 < w_n \end{cases}$$

$$c_\tau(w_n) = \begin{cases} \frac{4\pi}{(2S-1) w_n}\left[1 - w_n^2 \frac{2S^2 - 2S + 1}{16(2S-1)}\right], & w_n < w_1 \\ \exp\left(\sum_{j=0}^{3} p_{\tau,j} \ln^j w_n\right), & w_1 \le w_n \le w_2 \\ \frac{\gamma}{\sqrt{w_n}}, & w_2 < w_n \end{cases}$$

with $S(w_n) = 2.0022 - \ln w_n$, transition points $w_1 = 0.1$, $w_2 = 100$, amplitude $\gamma = 2$. The regularity involves the parameters $p_{n,0} = 1.6911$, $p_{n,1} = -6.7222 \cdot 10^{-1}$, $p_{n,2} = 3.3287 \cdot 10^{-2}$, $p_{n,3} = 3.5015 \cdot 10^{-3}$ and $p_{\tau,0} = 1.1552$, $p_{\tau,1} = -6.8479 \cdot 10^{-1}$, $p_{\tau,2} = 1.4884 \cdot 10^{-2}$, $p_{\tau,3} = 7.4966 \cdot 10^{-4}$. To be also applicable in the special case of a transversal incident flow $\mathbf{w} \parallel \boldsymbol{\tau}$ and to ensure a realistic smooth force $\boldsymbol{F}$, the drag is modified for $w_n \to 0$. A regularization based on the slenderness parameter δ matches the associated resistance functions r_n, r_τ (3) to Stokes resistance coefficients of higher order for $w_n \ll 1$, for details see [19].

Analogously, the (line) heat source acting on a slender body

$$q_{air}(s,t) = \mathcal{Q}(\mathbf{\Psi}(s,t), \mathbf{\Psi}_\star(\mathbf{r}(s,t),t))$$

$$\mathcal{Q}(\mathbf{\Psi}, \mathbf{\Psi}_\star) = 2k_\star\,(T_\star - T)\,\mathrm{Nu}\Big(\frac{\mathbf{v}_\star - \mathbf{v}}{\|\mathbf{v}_\star - \mathbf{v}\|} \cdot \mathbf{d_3}, \frac{\pi}{2}\frac{d\rho_\star}{\mu_\star}\|\mathbf{v}_\star - \mathbf{v}\|, \frac{\mu_\star c_{p\star}}{k_\star}\Big)$$

also depends on several material and geometrical properties as well as on the specific inflow situation. The number of dependencies reduces to three by non-dimensionalizing which yields the dimensionless Nusselt number Nu in dependence of the cosine of the angle of attack, Reynolds and Prandtl numbers. The Reynolds number corresponds to the relative velocity between air flow and glass jet, the typical length is the half jet circumference. The Nusselt number $\mathrm{Nu} : [-1,1] \times \mathbb{R}_0^+ \times$

$\mathbb{R}_0^+ \to \mathbb{R}_0^+$ is modeled as

$$\text{(4)}\quad \mathrm{Nu}(c,\mathrm{Re},\mathrm{Pr}) = (1-0.5\,h^2(c,\mathrm{Re}))\,(0.3+\sqrt{\mathrm{Nu}_{lam}^2(\mathrm{Re},\mathrm{Pr})+\mathrm{Nu}_{turb}^2(\mathrm{Re},\mathrm{Pr})})$$

$$\mathrm{Nu}_{lam}(\mathrm{Re},\mathrm{Pr}) = 0.664\mathrm{Re}^{1/2}\mathrm{Pr}^{3/2}$$

$$\mathrm{Nu}_{turb}(\mathrm{Re},\mathrm{Pr}) = \frac{0.037\,\mathrm{Re}^{0.9}\mathrm{Pr}}{\mathrm{Re}^{0.1}+2.443(\mathrm{Pr}^{2/3}-1)}$$

$$h(c,\mathrm{Re}) = \begin{cases} c\mathrm{Re}/\delta_h & \mathrm{Re}<\delta_h \\ c & \mathrm{Re}\geq\delta_h \end{cases}$$

where the regularization parameter δ_h ensures the smooth limit for a transversal incident flow in analogon to (3), [3].

The conservation of momentum and energy in (1)-(2) requires that the following relations are satisfied

$$\int_{I_V(t)} \mathbf{f}_{air}(s,t)\,\mathrm{d}s = -\int_V \mathbf{f}_{jets}(\mathbf{x},t)\,\mathrm{d}\mathbf{x}, \qquad \int_{I_V(t)} q_{air}(s,t)\,\mathrm{d}s = -\int_V q_{jets}(\mathbf{x},t)\,\mathrm{d}\mathbf{x}$$

for any arbitrary domain V and $I_V(t) = \{s \in I(t)\,|\,\mathbf{r}(s,t) \in V\}$. This implies distributional drag forces and heat sources in the balance equations of the air, i.e.

$$\mathbf{f}_{jets}(\mathbf{x},t) = -\int_{I(t)} \delta(\mathbf{x}-\mathbf{r}(s,t))\ \boldsymbol{\mathcal{F}}(\boldsymbol{\Psi}(s,t),\boldsymbol{\Psi}_\star(\mathbf{x},t))\,\mathrm{d}s$$

$$q_{jets}(\mathbf{x},t) = -\int_{I(t)} \delta(\mathbf{x}-\mathbf{r}(s,t))\ \mathcal{Q}(\boldsymbol{\Psi}(s,t),\boldsymbol{\Psi}_\star(\mathbf{x},t))\,\mathrm{d}s$$

with Dirac distribution δ. Considering k slender bodies in the air flow, we have $\boldsymbol{\Psi}_\mathbf{i}$, $i=1,...,k$ for every Cosserat rod. Assuming no contact between neighboring fiber jets, every single jet can be described by (1). Their multiple effect on the air flow is reflected in $\mathbf{f}_{jets}$ and q_{jets}, they become

$$\mathbf{f}_{jets}(\mathbf{x},t) = -\sum_{i=1}^{k}\int_{I_i(t)} \delta(\mathbf{x}-\mathbf{r}_\mathbf{i}(s,t))\ \boldsymbol{\mathcal{F}}(\boldsymbol{\Psi}_\mathbf{i}(s,t),\boldsymbol{\Psi}_\star(\mathbf{x},t))\,\mathrm{d}s$$

$$q_{jets}(\mathbf{x},t) = -\sum_{i=1}^{k}\int_{I_i(t)} \delta(\mathbf{x}-\mathbf{r}_\mathbf{i}(s,t))\ \mathcal{Q}(\boldsymbol{\Psi}_\mathbf{i}(s,t),\boldsymbol{\Psi}_\star(\mathbf{x},t))\,\mathrm{d}s.$$

2.2. Model simplifications for specific spinning set-up. In the considered rotational spinning process the centrifugal disk is perforated by a moderate number of rows with hundreds of equidistantly placed holes each (Figure 1). The spinning conditions (hole size, velocities, temperatures) are identical for each row. This special set-up allows for the simplification of the stated general model framework. We introduce a rotating outer orthonormal basis $\{\mathbf{a_1}(t),\mathbf{a_2}(t),\mathbf{a_3}(t)\}$ satisfying $\partial_t \mathbf{a_i} = \boldsymbol{\Omega}\times\mathbf{a_i}$, $i=1,2,3$, where $\boldsymbol{\Omega}$ is the angular frequency of the centrifugal disk. In particular, $\boldsymbol{\Omega} = \Omega\mathbf{a_1}$ and $\mathbf{e_g} = -\mathbf{a_1}$ (gravity direction) hold. Then, glass jets and air flow become stationary, presupposing that we consider spun fiber jets of certain length. In particular, we assume the stresses to be vanished at this length. Moreover, the glass jets emerging from the rotating device form dense curtains for every spinning row. As a result of homogenization, we can treat the air flow as rotationally invariant and each curtain can be represented by one jet. This yields an enormous complexity reduction of the problem. The homogenization together with the slender-body theory makes the numerical simulation possible, which involves the computation of only a few ($\approx$ 30–40) representative stationary fiber jets in a stationary two-dimensional air flow field, (for details see [3]). Disk geometry,

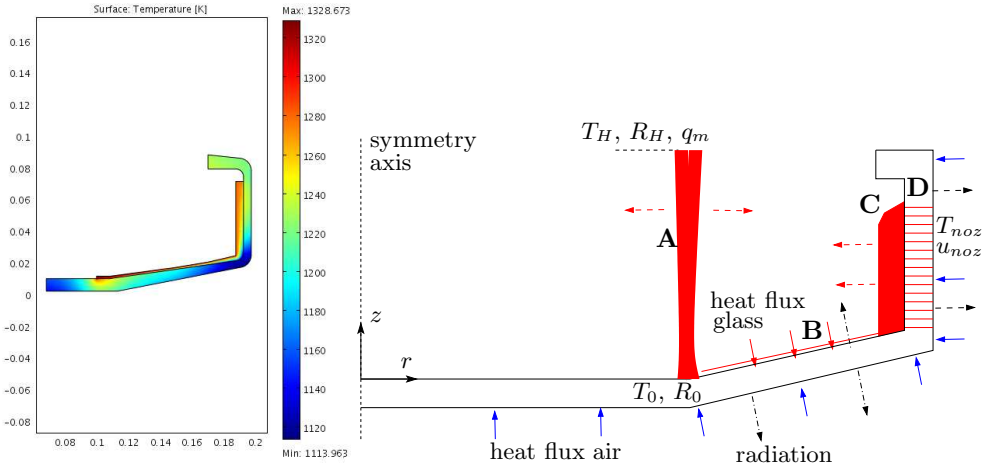

FIGURE 2. Melting phase. *Right:* Sketch of melt distribution (red) in the disk. A – glass string entering disk from stove, B – thin glass film, C – glass reserve (free surface flow), D – perforated wall with capillaries (pipe flows of glass). *Left:* Simulation of heat transfer in disk and glass reserve.

temperature at the disk wall and spinning conditions at the nozzles are in particular specified by the melting phase which we will study in the following.

3. Modeling of melting phase and disk mechanics

In the melting phase (Figure 2), a hot liquid glass string with known temperature and diameter enters the system. While falling down onto the disk it shrinks due to acceleration and cools down by radiation. Reaching the disk it starts creeping across the bottom driven by centrifugal and viscous forces. In front of the perforated wall it forms a reserve whose width is determined by an equilibrium of the hydrostatic pressure at the inlet of a capillary and its flow resistance. The disk deforms due to centrifugal forces and thermal expansion. Thereby, heat is exchanged with the glass melt, transferred by conduction and radiated into the cold environment.

The special industrial set-up allows the homogenization of the capillaries corresponding to a single spinning row. In the rotating basis $\{\mathbf{a_1}(t), \mathbf{a_2}(t), \mathbf{a_3}(t)\}$, the melt problem is then stationary and axially symmetric. The thermo-mechanics of the disk is described classically by linear elasticity theory with large deflections, thermal expansion and temperature-dependent material parameters and by heat transfer due to conduction and radiation towards an internal and an external temperature. The disk is attached to the glass reserve whose thermal model consists of heat conduction, convection and radiation. As these models are standard and can be solved together by the commercial software COMSOL, we do not go into details here. Instead we focus on the fluid dynamics of the glass melt that is characterized by thin layers and free surfaces. In the following we describe surrogate models for the melt distribution in the different parts of the disk (A-D, Figure 2) whose analytical results propagate directly into the thermo-mechanical disk-glass reserve problem, e.g. as boundary conditions, heat source, convection speed. The heat flux from the outer flow-fiber region into the disk is specified by the spinning phase.

A – Asymptotic model for the glass string provides Dirichlet boundary conditions

for the disk temperature. The glass string with mass flow q_m enters the system at a certain height $z = H$ with temperature T_H and radius R_H. Neglecting viscosity it obeys the principles of free fall with radiative cooling. The respective asymptotic one-dimensional balances yield the following result for the quantities at the disk surface ($z = 0$):

$$R_0 = R_H\Big(1 + 2\pi^2\rho^2 g H R_H^4/q_m^2\Big)^{-1/4}$$
$$T_0 = T_H\Big(1 + \frac{4\varepsilon\sigma q_m}{\pi c_p\rho^2 g R_H^3}T_H^3\left(\left(1 + 2\pi^2\rho^2 g H R_H^4/q_m^2\right)^{3/4} - 1\right)\Big)^{-1/3}$$

where ρ, c_p and ε are density, specific heat capacity and emissivity of glass, g is the gravitational acceleration and σ the Stefan-Boltzmann number.

B – Thin film approximation yields the inner heat flux from the glass into the disk. At the disk bottom the melt starts creeping towards the perforated wall driven by centrifugal and viscous forces. Thereby it forms a film which is much thinner than the disk wall. As radiation rises the effective heat conductivity of glass at high temperatures, the layer is also thermally thin. Thus, we can ignore temperature differences in the film normal to the surface with respect to those in the disk. Neglecting convective heat conduction in radial direction, balancing the heat flows leads to a Neumann boundary condition for the disk temperature $T_\diamond$,

$$k_\diamond\,\mathbf{n}\cdot\nabla T_\diamond = \varepsilon\sigma\left(T_{ref}^4 - T_\diamond^4\right) - \frac{c_p q_{\mathrm{m}}}{2\pi r}\,\boldsymbol{\tau}\cdot\nabla T_\diamond$$

where the normal $\mathbf{n}$ and tangential $\boldsymbol{\tau}$ vectors are given by the inclination angle of the planar disk surface, see Figure 2. Moreover, T_{ref} denotes an appropriately chosen mean temperature of all internal surfaces and $k_\diamond$ the heat conductivity of the disk.

C, D – Capillary pipe flow in conjunction with a Stokes flow simplification for the glass reserve yields the impact of the capillaries (heat source) on the disk, thickness of the reserve, its convection velocity and pressure on the disk as well as the conditions at the spinning nozzles. For a capillary we consider a pipe flow (flow through a hole) that is characterized by pressures and temperatures at the ends. Assuming that glass keeps essentially its temperature when passing a hole, we can conclude the z-dependent flow velocity u_{pw} at the perforated wall from the temperatures (as argument of viscosity ν) coming from the thermal reserve model

$$u_{pw} = \frac{n_\phi\,(n_z - 1)\,\Omega^2}{256\,\nu\,L_\diamond}\left(1 + \frac{W_\diamond}{2\,R_\diamond}\left(1 - \frac{h}{W_\diamond}\right)\right)\left(1 + \frac{h}{W_\diamond}\right)d_{noz}^4.$$

Here, u_{pw} describes the averaged velocity over the environment of a row of holes where d_{noz} denotes the hole diameter, n_ϕ, n_z the numbers of rows and columns of holes, $L_\diamond$ height of the perforated wall as well as $R_\diamond$ inner radius, $W_\diamond$ thickness and Ω angular frequency of the centrifugal disk. Note that u_{pw} depends on the thickness of the reserve h that is an unknown of the problem. The surrogate pipe model provides also the mass flow through the holes and the corresponding spinning conditions T_{noz}, u_{noz} at the outlet. The heat impact of the capillary flow on the disk can be represented by a heat line source.

Using u_{pw}, thickness h and dynamical flow quantities (pressure p, velocity (u, w) in radial and axial direction) of the reserve follow from a Stokes flow simplification. Starting from the Navier-Stokes equations for the free surface flow, a dimensional

analysis yields

$$\begin{aligned} & & \partial_r u + r^{-1} u + \partial_z w = 0 & & \\ \rho^{-1}\partial_r p - r\,\Omega^2 = 0, \qquad & & \rho^{-1}\partial_z p - \nu\left(\partial_{rr} w + r^{-1}\,\partial_z w\right) = 0 & & \\ & & u = u_{pw}, \qquad & w = 0 \quad & \text{on } \Gamma_{pw} \\ & u + \partial_z h\, w = 0 \qquad & \partial_r w = 0, \qquad & p = 0 \quad & \text{on } \Gamma_{free} \end{aligned}$$

where Γ_{pw} is the perforated wall and Γ_{free} the free surface. Assuming $h \ll R_\diamond$, this system can be reduced to a single differential equation for $j = h^4$:

$$\partial_{zz} j(z) = \frac{12\nu}{R_\diamond \Omega^2} u_{pw}(z; j), \qquad \partial_z j(z=0) = -\frac{6\nu q_m}{\pi \rho R_\diamond^2 \Omega^2} \text{ at inflow.}$$

The missing initial condition for j is replaced by the equality of inflow and outflow $q_m = 2\pi\rho R_\diamond \int_0^{L_\diamond} u_{pw}(z; j)\,\mathrm{d}z$. Pressure and convective velocity are then given analytically as functions of h (or j resp.).

4. Numerical treatment and results

The numerical solution of the melt-spinning process is characterized by the following four coupled routines:

- $(\Psi_{flow}, \Psi_{flux}) = \mathcal{S}_{air}(\Psi_{fiber}, \Psi_{temp}, \Psi_{mesh})$

The air flow simulation $\mathcal{S}_{air}$ depends on the impact of the fibers Ψ_{fiber} via the source terms, on the temperature of the disk walls Ψ_{temp} via the boundary conditions and on the mesh Ψ_{mesh} due to the varying geometry. The output Ψ_{flow} contains the information about the flow velocity, pressure, temperature, viscosity, thermal conductivity and heat capacity at each node of the mesh. The calculations are performed by using FLUENT, a commercial finite volume-based software by ANSYS, where a pressure-based solver is applied. To restrict the computational effort in grid refinement needed for the resolution of the turbulent air streams, a stochastic k-ω turbulence model can be considered. Such a modification of the model equations has no effect on the stated framework, where the jets-induced volume sources are incorporated by UDFs (user defined functions).

- $\Psi_{fiber} = \mathcal{S}_{jets}(\Psi_{flow}, \Psi_{nozzle}, \Psi_{mesh})$

The glass jets simulation $\mathcal{S}_{jets}$ depends on the fluid flow Ψ_{flow} via the source terms, on the melt conditions at the nozzle Ψ_{nozzle} via the boundary conditions and on the mesh because of the necessary interpolation and averaging procedures needed for the exchange of flow and fiber data [3]. The output Ψ_{fiber} contains the geometric, dynamic and thermic information of all glass jets. For the boundary value problem of the stationary Cosserat rod, systems of nonlinear equations are set up via a Runge-Kutta collocation method and solved by a Newton method in MATLAB 7.9. The convergence of the Newton method depends thereby crucially on the initial guess. To improve the computational performance the initial guess is adapted iteratively by solving a sequence of boundary value problems with slightly changed parameters. Details about the used continuation method can be found in [3, 4]. The representative glass jets are computed in parallel.

- $(\Psi_{nozzle}, \Psi_{temp}, \Psi_{def}) = \mathcal{S}_{disk}(\Psi_{flux})$

The combined thermodynamic disk and melt flow simulation $\mathcal{S}_{disk}$ depends on the heat flux across the disk wall Ψ_{flux} via the boundary conditions. It results in melt conditions at the nozzles Ψ_{nozzle} (i.e. temperature and outlet velocity), the temperature and the deformation of the disk walls Ψ_{temp}, Ψ_{def}. The computation of the creeping melt flow in the disk and through the capillaries is realized in MATLAB.

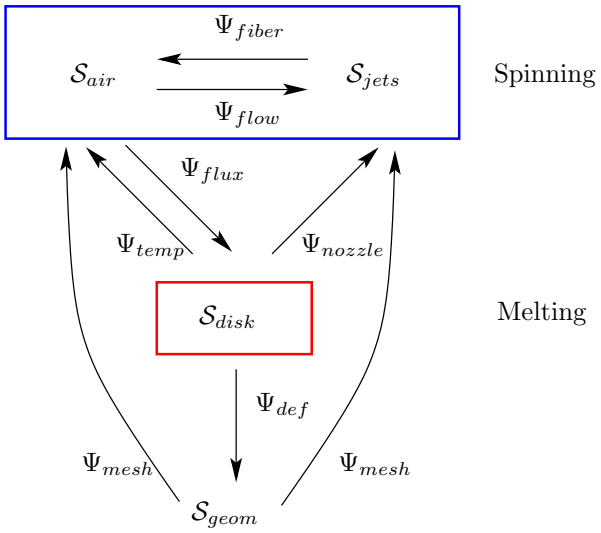

FIGURE 3. Coupling structure of the routines

It is attached to the simulation of the disk thermo-mechanics that is performed by using COMSOL, a commercial finite element software.

- $\Psi_{mesh} = \mathcal{S}_{geom}(\Psi_{def})$

The geometry computation $\mathcal{S}_{geom}$ for the fluid domain depends on the deformation of the disk walls Ψ_{def}. By help of the software GAMBIT a finite volume mesh Ψ_{mesh} is generated that is exported in two different formats: one for $\mathcal{S}_{air}$ (FLUENT) and one for $\mathcal{S}_{jets}$ (MATLAB).

The routines have a complex coupling structure as visualized in Figure 3, i.e. two-way coupling between $\mathcal{S}_{air}$ and $\mathcal{S}_{jets}$ via exchange models for momentum and energy (action-reaction principle), two-way coupling between $\mathcal{S}_{air}$ and $\mathcal{S}_{disk}$ via interface conditions at disk wall (continuity of temperature and heat flux), propagation of nozzle conditions from $\mathcal{S}_{disk}$ to $\mathcal{S}_{jets}$ and propagation of varying fluid domain / disk geometry from $\mathcal{S}_{disk}$ via $\mathcal{S}_{geom}$ to $\mathcal{S}_{air}$ and $\mathcal{S}_{jets}$. To realize this structure we use an algorithm that weakly couples the computations of the routines via iterations (Algorithm 1). For its stability it is important that $\mathcal{S}_{jets}$ is operating on consistent data coming from $\mathcal{S}_{air}$ and $\mathcal{S}_{disk}$. Therefore, $\mathcal{S}_{air}$ is computed twice per iteration step. The proposed procedure is adequate for the problem and has the advantage that we can combine well-established commercial software and self-implemented code.

Algorithm 1.

(1) *Initialize heat flux* Ψ_{flux}^{init} *by an educated guess and compute*

$$
\begin{aligned}
(\Psi_{nozzle}^{(0)}, \Psi_{temp}^{(0)}, \Psi_{def}^{(0)}) &= \mathcal{S}_{disk}(\Psi_{flux}^{init}) \\
\Psi_{mesh}^{(0)} &= \mathcal{S}_{geom}(\Psi_{def}^{(0)}) \\
(\Psi_{flow}^{(0)}, \Psi_{flux}^{(0)}) &= \mathcal{S}_{air}(\Psi_{temp}^{(0)}, \Psi_{mesh}^{(0)}) \ \textit{without jets} \\
\Psi_{fiber}^{(0)} &= \mathcal{S}_{jets}(\Psi_{flow}^{(0)}, \Psi_{nozzle}^{(0)}, \Psi_{mesh}^{(0)})
\end{aligned}
$$

(2) *Set* $k = 0$

(3) *Do the computations*

$$
\begin{aligned}
(\bullet, \Psi_{flux}^{k+1}) &= \mathcal{S}_{air}(\Psi_{fiber}^{(k)}, \Psi_{temp}^{(k)}, \Psi_{mesh}^{(k)}) \\
(\Psi_{nozzle}^{(k+1)}, \Psi_{temp}^{(k+1)}, \Psi_{def}^{(k+1)}) &= \mathcal{S}_{disk}(\Psi_{flux}^{(k+1)}) \\
\Psi_{mesh}^{(k+1)} &= \mathcal{S}_{geom}(\Psi_{def}^{(k+1)}) \\
(\Psi_{flow}^{(k+1)}, \bullet) &= \mathcal{S}_{air}(\Psi_{fiber}^{(k)}, \Psi_{temp}^{(k+1)}, \Psi_{mesh}^{(k+1)}) \\
\Psi_{fiber}^{(k+1)} &= \mathcal{S}_{jets}(\Psi_{flow}^{(k+1)}, \Psi_{nozzle}^{(k+1)}, \Psi_{mesh}^{(k+1)})
\end{aligned}
$$

update $k = k + 1$

while $\|\Psi_{fiber}^{(k)} - \Psi_{fiber}^{(k-1)}\| > tol$

Figures 4 and 5 show first results of our multimethods approach coupling melting and spinning phases. During the iterations, the geometry of the disk changes (Figure 4). As a consequence of its expansion the air gap for the burner flow shrinks which obviously affects the air flow and the jets dynamics. On the other hand, the jets forming a dense fiber curtain have a crucial impact on the flow field. For example the swirl velocity of the air flow is mainly caused by the pulling of the rotating curtain. These aspects were extensively studied and discussed in [3], see respective simulations and convergence results. The changes of the heat transport in the air flow influence the heat transfer into the disk, resulting in deflections of the disk walls and variations at the glass melt outlet.

In view of quality assessment, slenderness and homogeneity of the spun fiber jets play an important role. The diameters of the jets before they solidify are determined by the nozzle size and the extension (ratio of melt velocity at the nozzle and speed of the spun fibers), i.e. $d = d_{noz}\sqrt{u_{noz}/u}$. To produce slender fibers, the jets must thus lie in the fast axially directed air flow, as it is the case in Figure 5. Improvements are possible by modifications of geometry and process parameters, e.g. varying

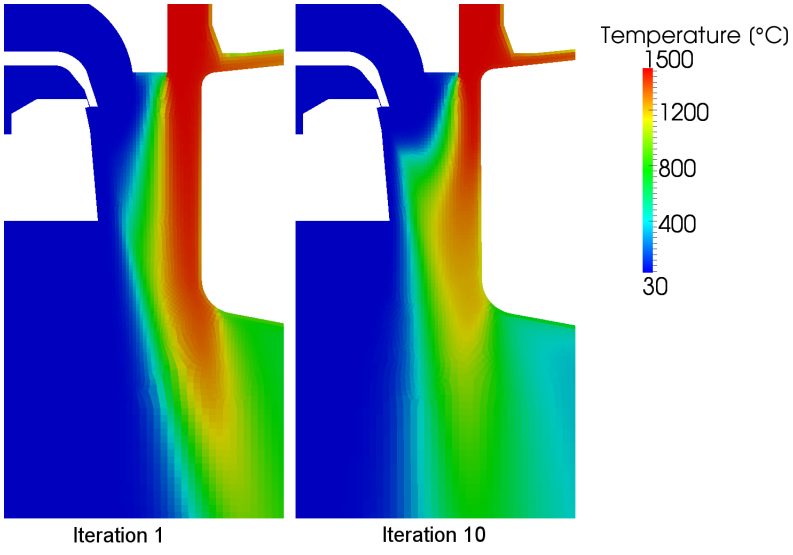

FIGURE 4. Air temperature in the iteration procedure of Algorithm 1. Zoom of the rotationally invariant flow in the region at the perforated disk wall.

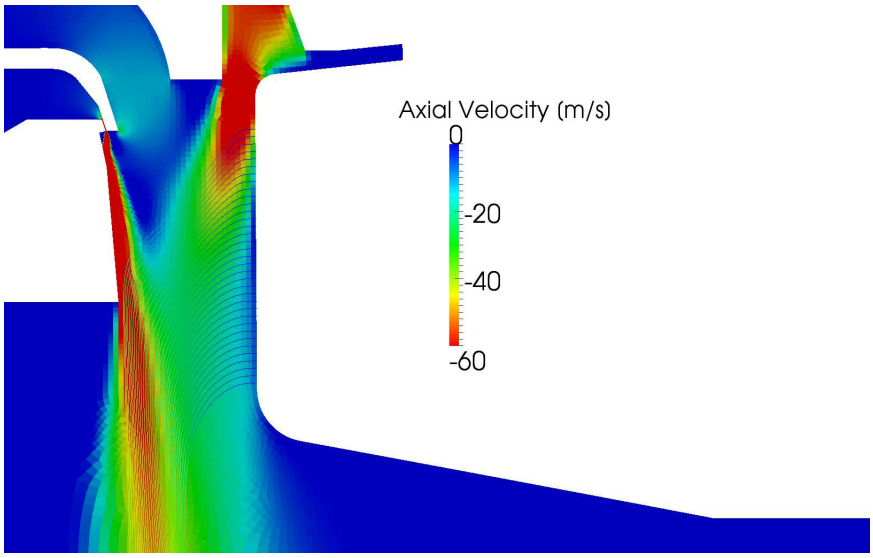

FIGURE 5. Final simulation result for glass jets and air flow. The color map visualizes the axial air velocity. In addition, immersed glass jet representatives are colored with respect to u.

pressure or mass flux at the inlet of the air streams. Homogeneity might result from different nozzle sizes. However, most of these modifications have a complex impact on the whole manufacturing process due to the delicate dependencies. Appropriate optimization strategies are left to future work.

5. Conclusion

The glass wool manufacturing process is a highly complex multiphysics problem whose simulation is a computational challenge. In this paper we have proposed a multimethods approach that is based on an asymptotic modeling framework. The algorithm weakly couples melting and spinning phases via iterations. The possibility of combining commercial software and self-implemented code yields satisfying efficiency off-the-shelf. Concerning its performance (robustness and convergence) further deeper investigations are required. However, the simulation results are very promising and demonstrate the applicability and practical relevance of our multimethods approach for ongoing optimization strategies of the glass wool production processes.

Acknowledgments

The authors would like to acknowledge their industrial partner, the company Woltz GmbH in Wertheim, Germany. This work has been supported by German Bundesministerium für Bildung und Forschung, Schwerpunkt "Mathematik für Innovationen in Industrie und Dienstleistungen", Projekt 03MS606 and by German Bundesministerium für Wirtschaft und Technologie, Förderprogramm ZIM, Projekt AUROFA 114626.

References

[1] S. S. ANTMAN, *Nonlinear Problems of Elasticity*, Springer, New York, 2006.

[2] W. Arne, N. Marheineke, A. Meister, and R. Wegener, *Numerical analysis of Cosserat rod and string models for viscous jets in rotational spinning processes*, Math. Mod. Meth. Appl. Sci., 20 (2010), pp. 1941–1965.
[3] W. Arne, N. Marheineke, J. Schnebele, and R. Wegener, *Fiber-fluid-interactions in rotational spinning process of glass wool production*, J. Math. Ind., 1 (2011), p. in press.
[4] W. Arne, N. Marheineke, and R. Wegener, *Asymptotic transition of Cosserat rod to string models for curved viscous inertial jets*, Math. Mod. Meth. Appl. Sci., 21 (2011), p. in press.
[5] G. K. Batchelor, *Slender-body theory for particles of arbitrary cross-section in Stokes flow*, J. Fluid. Mech., 44 (1970), pp. 419–440.
[6] R. G. Cox, *The motion of long slender bodies in a viscous fluid. Part 1. General theory*, J. Fluid. Mech., 44 (1970), pp. 791–810.
[7] L. J. Cummings and P. D. Howell, *On the evolution of non-axissymetric viscous fibres with surface tension inertia and gravity*, J. Fluid. Mech., 389 (1999), pp. 361–389.
[8] S. P. Decent, A. C. King, M. J. H. Simmons, E. I. Parau, I. M. Wallwork, C. J. Gurney, and J. Uddin, *The trajectory and stability of a spiralling liquid jet: Viscous theory*, Appl. Math. Mod., 33 (2009), pp. 4283–4302.
[9] J. N. Dewynne, P. D. Howell, and P. Wilmott, *Slender viscous fibers with inertia and gravity*, Quart. J. Mech. Appl. Math., 47 (1994), pp. 541–555.
[10] J. N. Dewynne, J. R. Ockendon, and P. Wilmott, *A systematic derivation of the leading-order equations for extensional flows in slender geometries*, J. Fluid. Mech., 244 (1992), pp. 323–338.
[11] V. M. Entov and A. L. Yarin, *The dynamics of thin liquid jets in air*, J. Fluid. Mech., 140 (1984), pp. 91–111.
[12] J. H. Ferziger and M. Perić, *Computational Methods for Fluid Dynamics*, Springer, Berlin, 3 ed., 2002.
[13] T. Götz, A. Klar, A. Unterreiter, and R. Wegener, *Numerical evidence for the non-existence of solutions to the equations describing rotational fiber spinning*, Math. Mod. Meth. Appl. Sci., 18 (2008), pp. 1829–1844.
[14] A. Hlod, *Curved Jets of Viscous Fluid: Interactions with a Moving Wall*, PhD thesis, Eindhoven University of Technology, 2009.
[15] A. Hlod, A. C. T. Aarts, A. A. F. van de Ven, and M. A. Peletier, *Mathematical model of falling of a viscous jet onto a moving surface*, Eur. J. Appl. Math., 18 (2007), pp. 659–677.
[16] ———, *Three flow regimes of viscous jet falling onto a moving surface*, arxiv:0811.2574, (2008).
[17] A. Klar, N. Marheinke, and R. Wegener, *Hierarchy of mathematical models for production processes of technical textiles*, ZAMM - J. Appl. Math. Mech., 89 (2009), pp. 941–961.
[18] N. Marheineke and R. Wegener, *Asymptotic model for the dynamics of curved viscous fibers with surface tension*, J. Fluid. Mech., 622 (2009), pp. 345–369.
[19] ———, *Modeling and application of a stochastic drag for fiber dynamics in turbulent flows*, Int. J. Multiphase Flow, 37 (2011), pp. 136–148.
[20] S. Panda, N. Marheineke, and R. Wegener, *Systematic derivation of an asymptotic model for the dynamics of curved viscous fibers*, Math. Meth. Appl. Sci., 31 (2008), pp. 1153–1173.
[21] E. I. Parau, S. P. Decent, A. C. King, M. J. H. Simmons, and D. Wong, *Nonlinear viscous liquid jets from a rotating orifice*, J. Eng. Math., 57 (2006), pp. 159–179.
[22] J. R. A. Pearson, *Mechanics of Polymer Processing*, Elsevier, 1985.
[23] N. M. Ribe, *Coiling of viscous jets*, Proc. Roy. Soc. London A, 2051 (2004), pp. 3223–3239.
[24] N. M. Ribe, M. Habibi, and D. Bonn, *Stability of liquid rope coiling*, Phys. Fluids, 18 (2006), p. 084102.
[25] N. M. Ribe, J. R. Lister, and S. Chiu-Webster, *Stability of a dragged viscous thread: Onset of 'stitching' in a fluid-mechanical 'sewing machine'*, Phys. Fluids, 18 (2006), p. 124105.
[26] H. Schlichting, *Grenzschicht-Theorie*, Verlag G. Braun, Karlsruhe, 1982.
[27] B. M. Sumer and J. Fredsoe, *Hydrodynamics around Cylindrical Structures*, World Scientific Publishing, 2006.
[28] G. I. Taylor, *Analysis of the swimming of long and narrow animals*, Proc. Roy. Soc. London A, 214 (1952), pp. 158–183.
[29] S. Tomotika, T. Aoi, and H. Yosinobu, *On the forces acting on a circular cylinder set obliquely in a uniform stream at low values of Reynolds number*, Proc. Roy. Soc. London A, 219 (1953), pp. 233–244.
[30] VDI-Gesellschaft, *VDI-Wärmeatlas*, Springer, 10 ed., 2006.

[31] I. M. Wallwork, S. P. Decent, A. C. King, and R. M. S. M. Schulkes, *The trajectory and stability of a spiralling liquid jet. Part 1. Inviscid theory*, J. Fluid. Mech., 459 (2002), pp. 43–65.
[32] A. L. Yarin, *Free Liquid Jets and Films: Hydrodynamics and Rheology*, Longman, New York, 1993.
[33] M. M. Zdravkovich, *Flow around Circular Cylinders, Vol 1: Fundamentals*, Oxford University Press, New York, 1997.

† FAU Erlangen-Nürnberg, Lehrstuhl für Angewandte Mathematik I, Erlangen, Germany
E-mail: `marheineke@am.uni-erlangen.de` (Corresponding author)

‡Fraunhofer-Institut für Techno- und Wirtschaftsmathematik, Kaiserslautern, Germany